TRAVELLING INTERPLANETARY DISTURBANCES DETECTED USING INTERPLANETARY SCINTILLATION AT 327 MHz

P. JANARDHAN*
Physical Research Laboratory, Ahmedabad, 380 009, India

V. BALASUBRAMANIAN
Radio Astronomy Centre, TIFR, P.O. Box 8, Udhagamandalam Ooty), 643 001, India

S. ANANTHAKRISHNAN
National Centre for Radio Astrophysics, TIFR, P.O. Box 3, Ganeshkhind, Pune, 411 007, India

M. DRYER
Cooperative Institute for Research in Environmental Sciences, University of Colorado, Space Environment Centre, NOAA, Boulder, CO 80303, U.S.A.

A. BHATNAGAR
Udaipur Solar Observatory, 11 Vidya Marg, Udaipur, 313001, India

P. S. McINTOSH
National Oceanic and Atmospheric Administration, Boulder, CO 80303, U.S.A.

(Received 23 September, 1994; in revised form 20 December, 1995)

Abstract. Based on the advance predictions of two flare-generated shock fronts, obtained from the Space Environment Centre (SEC, NOAA, Boulder), observations of interplanetary scintillation (IPS) were carried out with the Ooty Radio Telescope (ORT) on a grid of appropriately located sources during the period 31 October to 5 November, 1992. Solar wind velocities were derived by fitting model spectra to the observed spectra and two travelling interplanetary disturbances were detected. Both disturbances were traced back to an active region on the Sun which was located close to a large coronal hole. The roles of flares and coronal holes in producing such disturbances are examined and it is shown that in the present case both the coronal hole and the active region probably played key roles in generating the two IPS disturbances.

1. Introduction

The study of terrestrial effects of solar activity and variability has been a long standing problem and it has long been thought that intense geomagnetic storms and interplanetary disturbances (IPDs) can be traced directly to violent activity at active regions on the Sun (Watanabe and Marubashi, 1985; Schwenn, 1986; Dryer, 1994). In recent times claim has also been made that large transient events called coronal mass ejections (CMEs), rather than flares, may be the source of geomagnetic storms and other IPDs (Gosling, 1993). This claim is that the CMEs are associated solely with destabilization of large-scale coronal helmet structures and further, that flares play *no* fundamental role in CME generation. On the other hand, Dryer (1994) has suggested that flares do play a role in the spectrum of causes for generation of CMEs. Several techniques have been used during the past 4–5 decades for

* Currently on a Humboldt Fellowship at the Radioastronomisches Institut, D-53173, Bonn.

Solar Physics **166:** 379–401, 1996.

observing the outermost parts of the solar atmosphere, namely the corona and the solar wind. Each of these techniques is sensitive to only particular types of transients, and also probes only particular regions of the interplanetary medium (IPM). For a concise review of these techniques one may refer to Jackson (1991). *In-situ* measurements of the solar wind by the use of spacecrafts are generally confined to the ecliptic plane at 1 AU. The exception is the *Ulysses* spacecraft which has a flight path nearly perpendicular to the ecliptic plane. Spacecraft have also been used to probe the solar wind at distances less than 0.1 AU from the Sun by the use of techniques like Doppler scintillation, or Faraday rotation (Woo and Armstrong, 1981; Bird and Edenhofer, 1990). However, such measurements are infrequent. The only effective ground-based method of sampling the solar wind at all distances between 0.1 and 1 AU from the Sun, as well as off and on the ecliptic plane, is by using observations of interplanetary scintillations (IPS) of compact radio sources. Although a wealth of data has been obtained in recent decades by the use of all these techniques, regarding the occurrence of disturbances in the IPM and their associations with discrete ejections of mass and energy from the Sun, we are nowhere near a stage to confidently state that the cause-effect relationships of solar-terrestrial phenomena are well understood. In most of the investigations of the subject, attempts have been made with fair amount of success, in carrying out *ex-post facto* correlation studies of the different surface transient events on the Sun with the occurrences of geomagnetic disturbances.

In this paper we describe our observations of IPD by using the technique of IPS, based on real time predictions of the propagation of shock fronts triggered by solar flares. It may be noted that this is the second instance of the use of prediction-based observations. An earlier case of results from such a methodology of investigation has been reported by Manoharan *et al.* (1995).

2. The Shock Time of Arrival (STOA) Model

The function of the shock time of arrival (STOA) model is to model the propagation of IP transients. It is based on a series of 2-dimensional magnetohydrodynamic studies (2D MHD) of IP disturbances (Smith and Dryer, 1990, 1991). A detailed history of the development of the STOA model is given by Smart and Shea (1985). The operational code of the STOA model is initialized by:

– Real time observations of the optical location of a solar surface transient (usually Hα observations of a solar flare).

– Type II radio drift observations and Type II velocities from 75 MHz down to 25 MHz (the ionospheric cut-off) are combined with a coronal density model, based on plasma frequency emission at the fundamental mode, to provide an estimate of the shock velocity in the low corona. The centre of the shock is assumed to travel at this velocity.

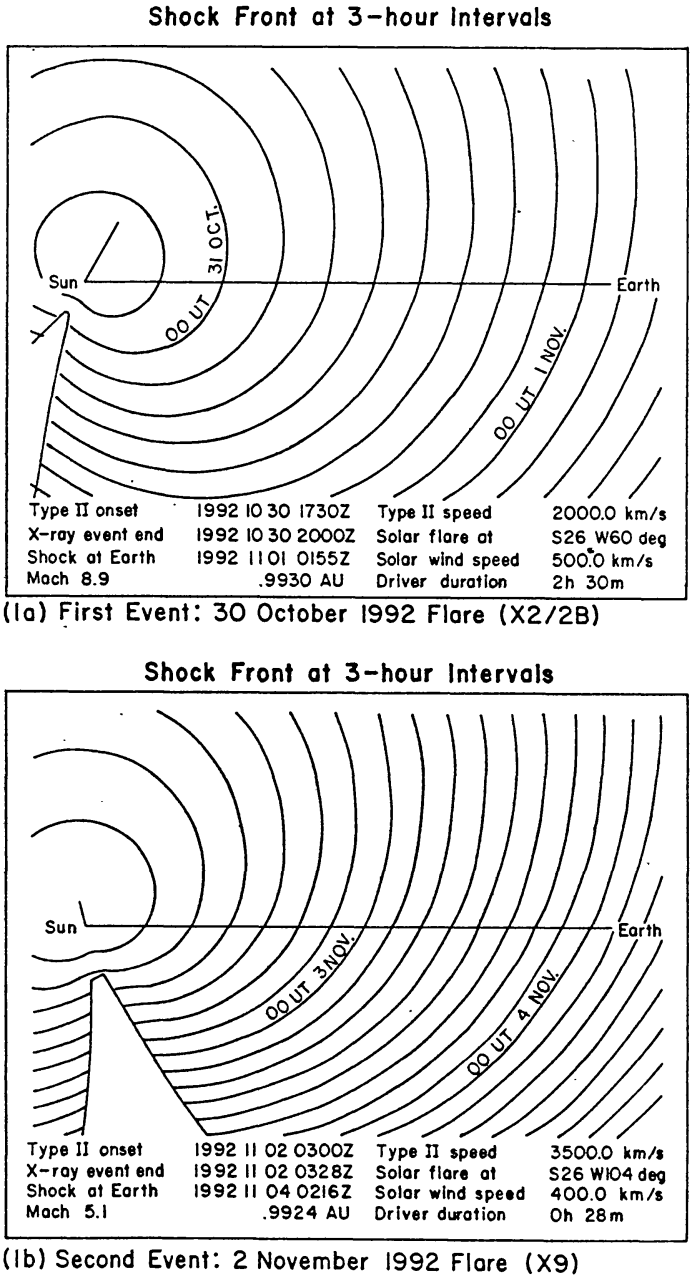

Figure 1. (a) Retrospective STOA plot showing the shock trajectory every 3 hours following the first flare event on 30 October, 1992 (see Section 2 for discussion). (b) Real-time STOA plot faxed to Ooty following the second flare event beyond the west limb on 2 November, 1992.

– A proxy estimate for a possible piston-driving duration, is taken to be the time interval between the first detection of the flare by the USAF Radio Solar Telescope Network (RSTN) observatories and the time at which GOES-6 or GOES-7 soft X-ray 0.1–0.8 nm flux decays to one-half the maximum flux level.

The STOA model is an assimilation of the 2D MHD results (cf., Smart *et al.*, 1986) so that only key kinematic results are provided. Thus neither the magnetic field nor the evolutionary dynamics of the shocked plasma are explicitly considered.

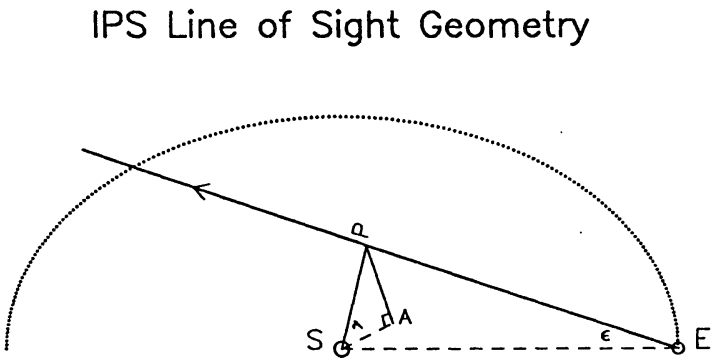

Figure 2. The relative Sun–Earth geometry in a typical IPS observation. The broken lines lie in the ecliptic plane, while the solid lines lie out of the ecliptic plane. The finely dotted line indicates the orbit of the Earth (marked by 'E') around the Sun (marked by 'S'). The thick solid line extending from E through the point P represents a typical line of sight to a compact radio source. The point P represents the point of closest approach of the line of sight to the Sun while the point A marks the footpoint of a perpendicular to the ecliptic plane from P. The angle ϵ is the solar elongation of the source while the angle γ is its heliographic latitude.

All of these properties can be computed only by a 3D MHD model. Figure 1(a) is a graphical summary of the predictions from the STOA model for the flare of 30 October, 1992, in region AR 7321. It shows the shock trajectory every three hours, plotted in the plane that contains the location of the flare and the Earth. The small tick mark at the flare location indicates the distance travelled through a pre-existing, representative, steady-state solar wind velocity profile, at the velocity suggested by the Type II shock velocity in the low corona. The shock, initially piston driven (as indicated by the tick mark's length), is thereafter assumed to decay as a classical blast wave with velocity proportional to $R^{-1/2}$ that rides over the background solar wind (R being the distance from the Sun). The shape of the shock is taken as an empirically-based cosine squared function (Smart *et al.*, 1986) that assumes (as shown by the MHD solutions) a gradual decay along the flanks. The curves in Figure 1(a) are terminated at each clock time (every three hours) to both the east and west of the flare site when the shock decays to the local magneto acoustic speed, $M_A = 1.0$. Physically, the hitherto entropy-generating shock, caused by the nonlinear steepening of fast-mode MHD waves, loses this function as it decays, or gets smeared out, into a *linear* fast-mode wave. Thus MHD waves are assumed to extend within the 'V' line, and hence, are ineffective in causing a geomagnetic disturbance, if the Earth were located therein.

3. Single Station IPS Observations and the Determination of Solar Wind Velocities

IPS is a diffraction phenomenon in which coherent electromagnetic radiation, from a distant radio source, passes through the solar wind, which is a turbulent refracting medium, and suffers scattering. This results in random temporal variations of the

signal intensity (scintillation) at the Earth. The geometry of the line of sight (LOS) to the compact radio source with respect to the Sun (marked by 'S') and the Earth (marked by 'E') is shown in Figure 2. The broken lines in Figure 2 lie in the ecliptic plane, while the solid lines lie out of the ecliptic plane. The finely dotted line indicates the orbit of the Earth around the Sun. The point 'P' represents the point of closest approach of the LOS to the Sun, while the point 'A' is the foot point of a perpendicular from P to the ecliptic plane. The thick solid line extending from the E through P represents a typical LOS to a compact radio source. The angle ϵ is the solar elongation of the source while the angle γ is its heliographic latitude. IPS is highly sensitive to turbulence in the solar wind. When travelling IP transients cross the LOS to the source they exhibit themselves as enhanced levels of scintillation; i.e., higher than expected scintillation index (m), where m is the ratio of the root mean-square deviation of signal intensity to the mean signal intensity. In simple terms one may state that if we detect an IPD travelling towards the Earth by using the technique of IPS, we can be forewarned about its possible effect on the Earth at a later time.

IPS can be used to study changes in the large-scale structure of the interplanetary medium (IPM) by detecting and tracking interplanetary disturbances as they propagate in space. This is achieved by observing a large number of sources all over the sky and mapping the activity in the IPM (Gapper *et al.*, 1982; Hewish, Tappin, and Gapper, 1985; Hewish and Duffett-Smith, 1987; Manoharan *et al.*, 1995) by noting the enhancements $g = \Delta S/\overline{\Delta S}$ for each observation. Here ΔS is the scintillating flux of the source while $\overline{\Delta S}$ is the long-term mean scintillating flux of the source. On such maps, called 'g-maps', enhanced density regions in the IPM will show up as regions of $g > 1$ while depleted density regions will show up as regions with $g < 1$.

Traditionally, IPS measurements at meter wavelengths were made by using large dipole arrays operating as transit instruments. In some cases they were used only to measure the scintillation indices of the sources. Measurements of solar wind velocity required a network of at least three telescopes with baseline separations approximately equal to the fresnel distance at the observing frequency (Kakinuma *et al.*, 1973; Kakinuma and Kojima, 1984; Alurkar *et al.*, 1989). It has recently been shown (Manoharan and Ananthakrishnan, 1990) that reliable estimates of solar wind velocities and angular diameters of compact components of radio sources can be obtained from observations with a single telescope. This is achieved by fitting model spectra to the observed IPS spectra. The model depends on the variations in a number of parameters like power-law index, axial ratio of the irregularities, source size, random velocity component and most importantly, a knowledge of the smallest scale sizes present in the IPM. This scale size known as the inner-scale, represents a spatially dissipative scale length below which there is little IPS power, due to the absence of smaller irregularities. IPS observations (Coles, 1978; Scott, Coles, and Bourgois, 1983; Manoharan, Ananthakrishnan, and Pramesh Rao, 1987), and spacecraft experiments (Yakovlev *et al.*, 1980) showed that this

scale size attenuates the IPS power spectrum at high temporal frequencies in a manner similar to the effects of the source size cut-off. Hence, differentiating between source size effects and effects caused by the inner-scale depended upon reliable estimates of source size, which eventually came from very long baseline interferometry (Ananthakrishnan *et al.*, 1989). Once the medium was calibrated to determine the inner-scale, the model was capable of making reliable estimates of solar wind velocities and source sizes, for spectra with good signal to noise ratio (S/N). A low S/N would cause the source size to be unreliable as the high-frequency portions of such spectra will be contaminated by noise.

The scintillation index (m) of a source increases with decreasing solar elongation (ϵ) until a certain ϵ. After this point it shows a broad turnover and then falls off sharply with further reduction in ϵ. This ϵ at which the m turns over is dependent on frequency and at 327 MHz it lies between 10° and 15°. The region at ϵ larger than the turnover defines the region of weak scattering where the approximation of scattering by a thin screen is valid (Salpeter, 1967).

The Ooty Radio Telescope (ORT), operating at 327 MHz, used for the IPS observations described in this paper, is capable of carrying out IPS observations of about 150 to 200 sources in a single day (Selvanayagam *et al.*, 1993). An IPS survey was initiated in August 1992 (Balasubramanian *et al.*, 1993) to detect compact sources in the 7 steradian of the sky visible to the ORT. The principal aim of the IPS survey was to rapidly compile a list of sources having compact enough components which would exhibit IPS, such that they are well distributed spatially. To achieve this aim, it was decided to observe all the sources from the Texas and Molonglo catalogues of radio sources (Ghigo and Owen, 1978; Large *et al.*, 1981) having flux density larger than 1.5 Jy, and then prepare a list of those sources alone which showed strong IPS at 327 MHz. All the 5000 sources shortlisted for the IPS observations were not expected to scintillate. As the scintillation survey progressed it was apparent that one could expect a total of 1000 to 1500 sources from the list to be good scintillators at 327 MHz. Analysis of data from the IPS survey is currently in progress and hence the compilation of the list of scintillators is yet to be completed. During the survey the signal intensity from each of the sources was recorded for a duration of three minutes. In order to carry out the survey effectively and rapidly, the ORT was parked at an hour angle and the direction of the beam of the telescope was changed in declination, such that sources with larger right ascensions were observed at progressively later epochs. The east–west half-power beam width of the ORT is about 2.2° (HPBW), which readily enabled the acquisition of three minutes of data on each source as it transited the beam.

The ORT was used in the correlation mode during the survey observations (correlation of signals from the north and south halves of the telescope). From the master list of 5000 sources, only those sources lying to the east of the Sun–Earth line, and in the elongation range $10° < \epsilon \leq 55°$ were chosen for observations on a given day. These limits of ϵ are such that below the lower limit one would have strong scattering conditions in the IPM, and beyond the upper limit of ϵ there

would not be any appreciable IPS even for compact enough sources, owing to the very low fluctuations in density of the electrons in the solar wind. For observations within these limits of ϵ, the distance from the Sun to the LOS to the source was in the range of 0.2 to 0.8 AU.

At each stationary setting of the ORT in hour angle, it took a maximum of about 2.5 hours to observe 50 sources. The sequence of observations was such that, at each setting of the telescope, sources with lesser ϵ were observed at progressively later epochs of time. The list of sources selected for the survey contained many sources with close enough right ascensions, but separated in declination; hence it required several settings of the ORT on each day of observation to have a look at all the sources.

During the observations, data from an off-source region was also recorded at intervals of about half an hour. A calibration source was also monitored at the beginning and end of the observations to determine the sensitivity of the telescope. Gain variations in the telescope, if any, were monitored by simultaneously recording data from an adjacent beam which was pointing away from the source. This off-source beam also helped in identifying terrestrial interference.

The time scale of IPS at 327 MHz is around 0.1 s. The data was therefore integrated for 50 ms, sampled at 20 ms intervals and stored on the computer in blocks of 2600 measurements of intensity points corresponding to 52 s of data. Each source was observed for about three minutes and the spectra of each 52 s block of data was integrated and averaged. This averaged power spectrum was then corrected for the effects of the time constant response and stored in the computer. The ratio of the r.m.s. of the scintillation to the difference between the on-source and off-source mean, m, is then calculated. The final stage in the data reduction consisted of fitting all the observed spectra having good S/N ($\geq$ 15 db) with model spectra to determine solar wind velocities and source sizes. It may be noted that the method of determining the solar wind velocity by using the single-station method of IPS observations is valid (strictly speaking) only for quiescent or quasi-steady state solar wind. This is due to the fact that the single station IPS method is based on a simplified model of the steady solar wind. However, transient conditions of the solar wind (such as the case of a high speed stream of solar wind crossing the LOS to IPS sources) are comparatively rare, except at the epochs corresponding to the maximum of the solar activity cycle. Under such disturbed conditions, the power spectrum of intensity fluctuations due to IPS can deviate considerably from the predictions of the steady-state model. Nevertheless, the single station IPS method is useful in determining the higher than average values of the speed of the solar wind, with a precision of ± 50 km s^{-1} even for disturbed conditions of solar wind.

4. The STOA Predictions and the Detection of the IPD

4.1. The flares of 30 October and 2 November, 1992

A strong flare of class X2/2B began at 16:59 UT on 30 October, 1992. The Hα maximum occurred at 17:30 UT and the X-ray flux peaked at 18:16 UT. The flare occurred in the active region AR 7321 located at S25 W60 (S25 L71 in Carrington coordinates). Type IV radio broadband emission, starting at 17:30 UT, was observed at Sagamore Hill; this emission possibly obscured any Type II radio drift which, then, had to be assumed for the purpose of the real-time shock velocity input for the STOA model as discussed below. This flare was accompanied by impulsive emission at 2.7 GHz, with a peak intensity of 7700 solar flux units (s.f.u.), and lasted more than three hours. Based on the characteristics of the flare observed in real time, inputs were made to the STOA model (see Section 2) by the co-authors of this paper located at the Space Environment Centre at Boulder, Colorado, of the National Oceanic and Atmospheric Administration (SEC, NOAA). The STOA model predicted the passage, around 05:30 UT on 31 October, 1992, of a strong shock west of the Sun–Earth line at an ϵ of about 24°. The predictions of the STOA model were immediately faxed to the observatory at Ooty. Based on this advanced intimation IPS observations in the survey mode were started with the ORT from 01:20 UT on 31 October, 1992. In contrast to the normal survey mode (in which only sources lying to the east of the Sun were observed) the grid of radio sources selected for the IPS observations in this case were located to the west of the Sun (in keeping with the STOA prediction) in the ϵ range $10° < \epsilon < 55°$. The observations were carried out for six days, from 31 October, 1992 to 5 November, 1992. Each day's observing session lasted for about 10 hours.

Another very strong flare also occurred in the same active region AR 7321 on 2 November, 1992 at 03:08 UT. This flare erupted behind the west limb of the Sun. Predictions of travelling IPD were made by SEC, NOAA by using the STOA model in the case of this flare also and the information was faxed immediately to Ooty. As discussed in more detail in the forthcoming sections, the propagation of the IP disturbances triggered by each of the two flares were unambiguously detected during the IPS observations with the ORT, as they crossed the lines of sight to the observed radio sources. The flare of 2 November was a long duration (44 minutes) X9 flare and caused a peak emission of 5000 s.f.u. at 2.7 GHz. Radio bursts of both type II and type IV associated with this flare were detected. The radio telescope patrol of the Culgoora Ionospheric Prediction Services reported the Type II shock velocity to be 3500 km s^{-1}. Although this appears to be somewhat high, this was used as input to the STOA model.

The input parameters, used in *real time* for this *first* event, were as follows:

(1) Initial shock velocity was taken to be 2000 km s^{-1} on the assumption that the Type II onset and drift (at either the fundamental plasma wave frequency or its

second harmonic) started at 17:30 UT on 30 October, 1992 but was obscured by the intense Type IV broadband emission.

(2) Driving piston duration was assumed to be 1.5 hr, based approximately on the proxy soft X-ray duration (as described above).

(3) Background solar wind velocity was assumed to be 400 km s^{-1}, independent of heliolongitude, at 1 AU.

As noted earlier, the STOA model predicted shock passage on 31 October, 1992 at a benchmark ϵ of about 24° west of the Sun at around 05:30 UT, for the above values of input parameters.

The STOA input parameters, used in *real-time* for the *second* event, were as follows:

(1) Initial shock velocity of 3500 km s^{-1} as provided by the Culgoora radio observatory.

(2) Driver duration 28 min, suggested by the soft X-ray profile from the flare at S26 W104.

(3) Background solar wind velocity of 400 km s^{-1}.

For the above values of input, the STOA model predicted shock passage at an ϵ of about 35° west of the Sun by about 02:00 UT on 3 November, 1992, as shown in Figure 1(b).

It may be noted that in the case of both flares there were high energy (> 100 MeV) proton events detected by the GOES-7 satellite. For the flare of 30 October, 1992 proton detectors on board GOES-7 registered an increase of two orders of magnitude, with the peak flux being 2700 proton flux units (p.f.u.) (*Solar Geophysical Data (SGD)*, 3 November, 1992). For the second flare the proton event began at 05:20 UT, peaked at 120 p.f.u. at 05:45 UT and ended at 06:00 UT (*SGD*, 10 November, 1992). The previous flare of greater magnitude was a flare of class X12 on 11 June, 1991.

4.2. The Detection of IP Transients by Velocity Mapping

On each of the six days of observations the number of IPS sources observed were 92, 157, 148, 122, 143, and 69, respectively. From this data good estimates of velocities and source sizes were obtained for 41, 64, 40, 45, 46, and 15 sources, respectively. The day to day observations were not on the same sources. Data on all the sources did not give velocities and sizes because not all the sources were scintillators.

The measured values of solar wind velocities are presented in Figure 3 as a 'spatial map of velocities' or V-map. In this figure the Sun's location is at the center of the concentric semi-circles. Measurements lying along a given semi-circle are from sources having the same ϵ. The values of the elongations corresponding to each of the semi-circles are indicated in the figure. Also indicated in each V-map is the corresponding date of observation. In the figure, velocities $\leq$ 600 km s^{-1} are shown by small filled circles, while velocities > 600 km s^{-1} are shown by open

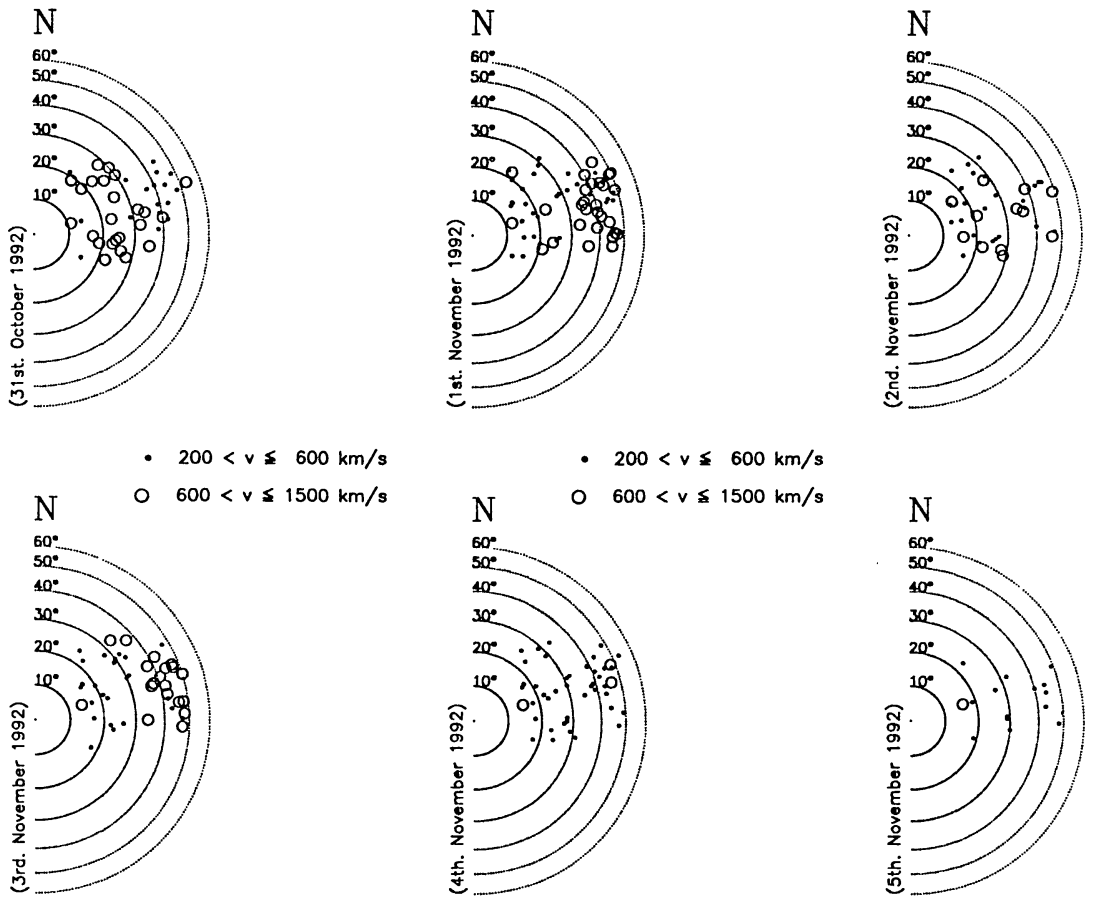

Figure 3. Solar wind velocity maps (V-maps) for each of the six days of observation. The finely dotted semi-circles are loci of equal ϵ with the Sun located at the center. The small filled circles represent solar wind speeds in the range 200 km $s^{-1} < V \leq 600$ km s^{-1}, while the open circles represent velocity values in the range 600 km $s^{-1} < V \leq 1500$ km s^{-1}. The location of each point is given by the position angle, measured north through east, of the solar wind across the source. North is marked at the top of each map by a large 'N'. Also indicated on each map is the corresponding date of observation.

circles. The position of each point in the V-map is fixed by the position angle of the line joining the Sun and the source in a plot of right ascension vs declination in rectangular Cartesian coordinates. The position angle is measured from north through east. North is indicated at the top of each map by a large 'N'. For the data of 31 October, 1992 (Figure 3) it is seen that the high values of solar wind velocity are grouped in the range of ϵ between 15° and 35°; lower values lie in the range 35° and 55°. We may recall that the sequence of observations is such that sources at smaller values of ϵ, at each setting of the ORT, are observed at later epochs. Hence the velocity map of 31 October shows that the propagating IPD was intercepted during the course of the observations as the lines-of-sight to the sources continually shifted closer to the Sun. This is seen clearly in Figure 4 which is a scatter plot of velocity as a function of time on 31 October, 1992. The broken line in Figure 4 is marked at a velocity of 600 km s^{-1}. In keeping with the STOA model prediction,

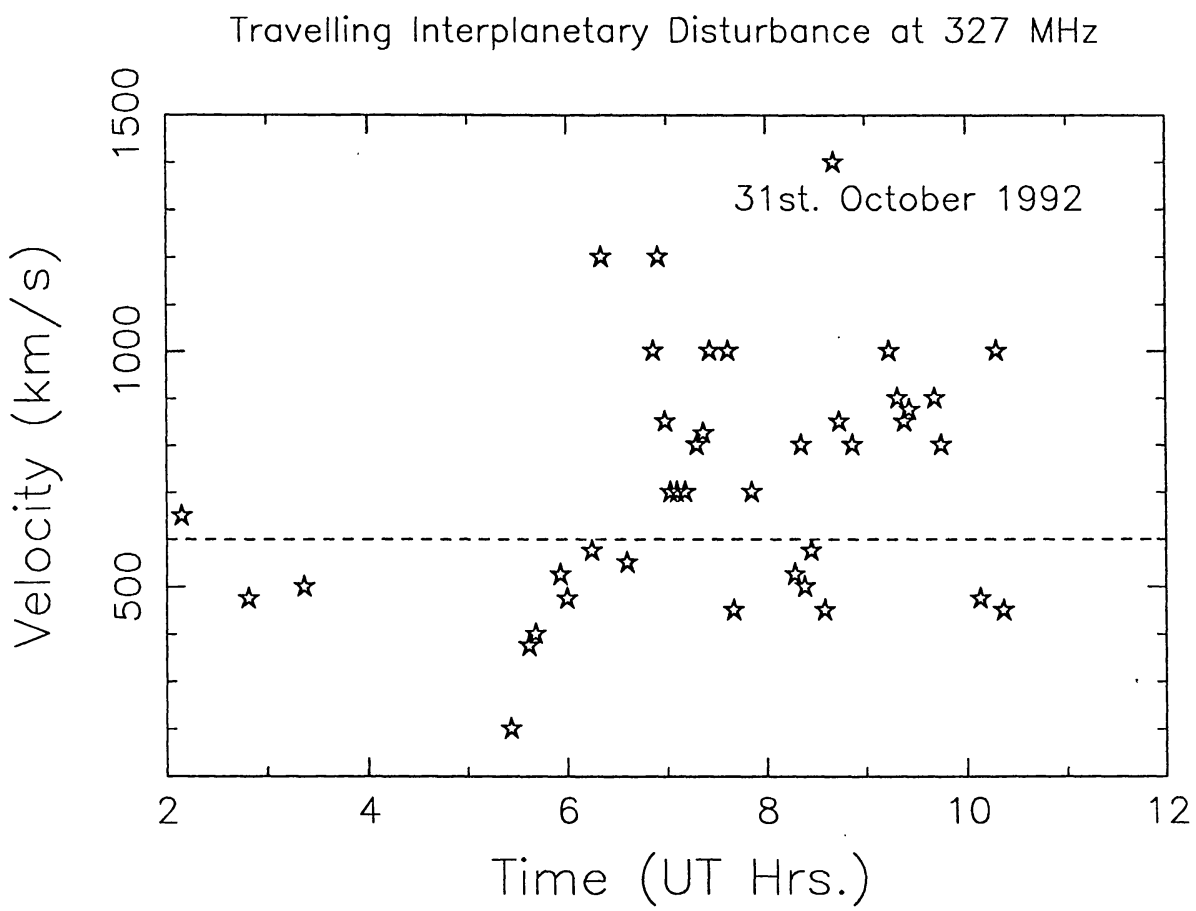

Figure 4. A scatter plot of solar wind velocity as a function of time in UT for the observations of 31 October, 1992. The broken line is marked at a value of velocity = 600 km s^{-1}. Note the abrupt jump in velocities around 06:15 UT.

there is an abrupt jump in the velocities at about 06:15 UT. The ϵ of the LOS at this time corresponds to 35°. From Figure 4 it is seen that the velocities remained high till about 10:25 UT on 31 October at which time the IPS observations for the day came to a close. The time interval between the onset of the flare on 30 October and the observed jump in velocities on 31 October, is $\sim$ 13 hours. Hence we conclude that the high velocity front was initiated by the flare of 30 October and it travelled at an average speed of $\sim$ 1800 km s^{-1} to cover a distance of about 0.57 AU (corresponding to $\epsilon = 35°$).

The V-map of 1 November, 1992 (Figure 3) shows that the high velocities are present mostly at $\epsilon > 35°$. The temporal sequence of the measurements for this day show that except for a few points, the velocities were normal at $\epsilon < 35°$ irrespective of the time at which the measurements were made. The conclusion is that the observations on this day are essentially detecting the trailing edge of the velocity transient as it moved beyond the upper ϵ limit of the observations. Although we did not have observations from 10:25 UT on 31 October to 00:00 UT on 1 November, it is quite likely that the high velocity winds were sustained throughout this interval. The V-map of 2 November, 1992 (Figure 3) shows a

somewhat uniform spatial distribution of high and low velocity points. Also to be noted is the fact that although the total number of sources observed on 2 November, 1992 are nearly equal to the number observed on 1 November, 1992 (148 vs 151) the proportion of scintillators (an indicator of enhanced activity) on 2 November are much less compared to the earlier two days (40/148 vs 41/92 and 64/157). Clearly, the data of 2 November, 1992 indicate the return of quiescent conditions in the IPM after the passage of the IPD.

The V-map for 3 November, 1992 (Figure 3) also shows the trailing edge of a high velocity event travelling across the lines-of-sight. This is seen by the well-defined separation of high velocities occurring beyond $\epsilon = 35°$, and lower velocities at $\epsilon < 35°$. The earliest of the high velocity measurements on this day was at 01:58 UT at an ϵ of 48°. The interpretation of the results is that the flare at 03:08 UT on 2 November, 1992 triggered an IP transient propagating at high velocity which had travelled beyond the LOS at $\epsilon = 35°$ by about 02:00 UT on 3 November, 1992. The estimated average speed of the transient would thus be $\sim$ 1050 km s^{-1}. This result was also in keeping with the STOA prediction as discussed in Section 2.

The V-map of 4 November, 1992 shows normal velocities all over $15° < \epsilon < 52°$. There are only three points with velocity just beyond 600 km s^{-1}. The data is similar for 5 November, 1992 although there are fewer measurements on this day as compared to that on 4 November, 1992.

5. The g-Maps

Figure 5 shows maps of the scintillation enhancement factor 'g' for each of the six days of observations. Similar to the V-maps, the dotted concentric semi-circles are semi-circles of constant ϵ with the Sun located at the centre. The g-values on each day are shown by two different markers, with the large open circles indicating 'g' in the range $1.20 < g \leq 3.0$, and the small filled circles indicating 'g' in the range, $0.0 < g \leq 1.20$. The position of each point on the map is given by the position angle of the source. North is marked by a large 'N' at the top of each map. Also indicated on each map is the date of the observation.

Values of 'g' for each observation were computed using the relation

$$g = \frac{m_{\text{obs}}}{m_{\text{theo}}},$$

where m_{obs} is the observed scintillation index at a given ϵ and m_{theo} is the scintillation index computed at the same ϵ using a power-law model (Marians, 1975). It assumes that the solar wind irregularity spectrum is a power law with an index of 3.3. The source size used in each computation of m_{theo} was that derived from the model fit to the observed spectra.

This method is in contrast to the Cambridge g-maps where a very large number of observations, at various elongations, on each source is used to compute a

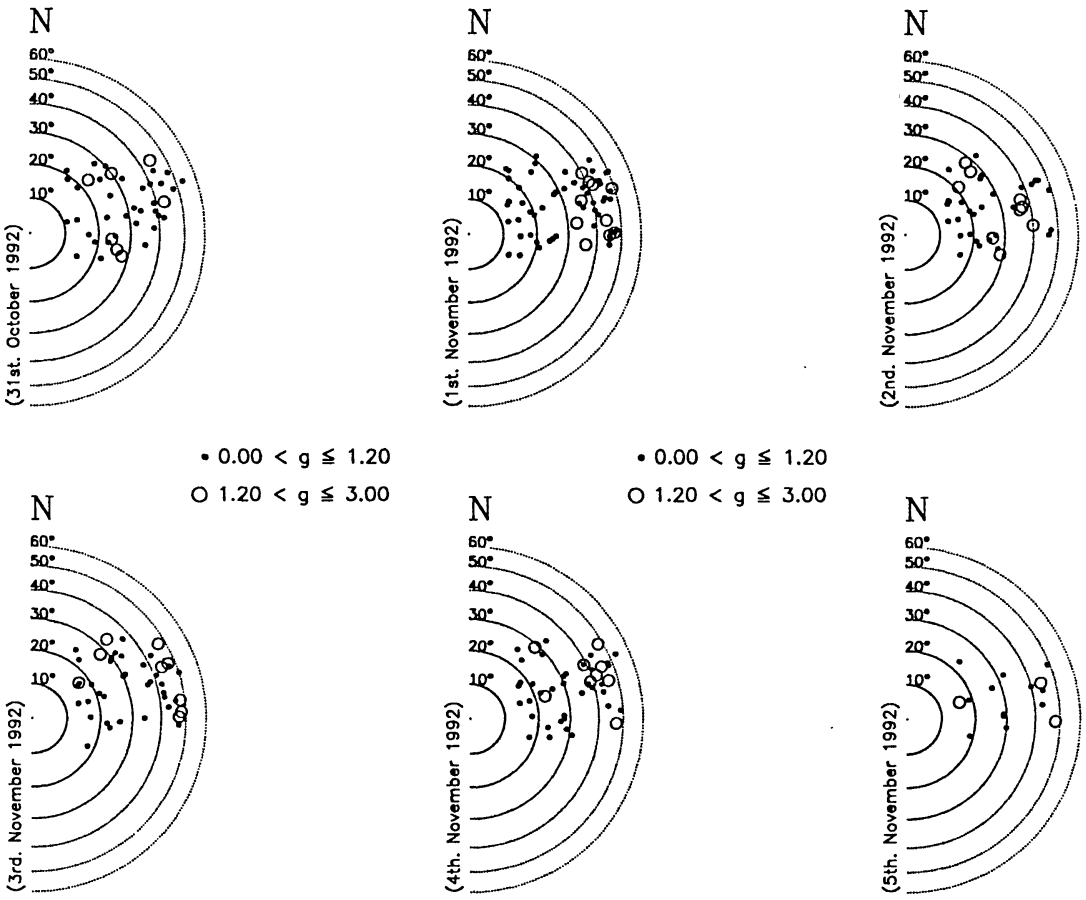

Figure 5. Maps of scintillation enhancement factor (g-maps) for each of the six days of observation. The finely dotted semi-circles are loci of equal ϵ with the Sun located at the center. The small filled circles represent 'g' values in the range $0.0 < g \leq 1.2$, while the open circles represent 'g' values in the range $1.2 < g \leq 3.0$. The location of each point is given by the position angle, measured north through east, of the solar wind across the source. North is marked at the top of each map by a large 'N'. Also indicated on each map is the corresponding date of observation.

normalization factor for each observation. Our g-values are therefore somewhat imprecise, but can be improved as more and more observations are made on each source over a period of time. A comparison of the g-maps and V-maps on a day to day basis (Figure 5 and Figure 3) indicates that it would have been difficult to detect the two transients with the g-maps alone, except possibly for the g-maps of 1 and 3 November, 1992. On these days (Figure 5) the high 'g' region at larger ϵ is fairly distinct from the low 'g' region at smaller ϵ. However, in view of the inaccuracies inherent in the determination of the g-values reported here caution is to be exercised in interpreting the g-maps.

6. Events on the Solar Surface

Figure 6 is the partial synoptic chart for the solar surface features which were observed during the period of our interest. This synoptic map is substantially improved from the preliminary version published in the NOAA preliminary *Report and Forecast of Solar-Geophysical Activity* and was produced after carefully re-examining the relevant Hα pictures taken during the period of interest. In Figure 6, dates of central meridian passage at the top refer to the corresponding solar longitude at the bottom. Negative polarity is shaded light grey while positive polarity is shown white. Coronal holes are shaded dark grey and have the polarity of the surrounding solar surface. Large sunspots observed in Hα are shown by large dots while bright chromospheric plages are indicated by areas of small dots. Areas with diagonal lines overlying spots and plage indicate occurrence of strong X-ray flares. Dark filaments are marked by irregular, cross hatched areas along some of the lines of polarity reversal near important active regions.

Attention is to be mainly focussed on the active region AR 7321 (at heliographic longitude 71° and latitude 25° south) as well as the coronal hole seen adjacent to it. The flares of 30 October and 2 November occurred in this active region. Region AR 7321 emerged on the visible disk of the Sun on 23 October, 1992, and grew more rapidly than any other sunspot group present during that solar rotation (Carrington rotation No. 1861) and became exceptionally large and complex in just 48 hours. This large region, unlike other significant regions on this rotation (CR 1861), formed away from pre-existing boundaries in the large-scale magnetic fields. Filaments also formed in a semi-circle around the sunspot group early in its development. The filament on the left (east) boundary rotated to the east and extended towards the small and weak cell of negative polarity north of the region, possibly merging with it by the time of the flare events. This evolving filament is indicated in Figure 6 as a double filament at the left edge of AR 7321.

The largest low latitude coronal hole during CR 1861 lay only 10° east (left) of the active region AR 7321 (Figure 6). Spectroheliograms taken in He I line ($\lambda = 10830$ Å) during the period 26–30 October, 1992 showed that the area of this coronal hole decreased, while it became brighter, showing more contrast with the surrounding areas. At the same time the area of AR 7321 increased from 60 millionths of the solar hemisphere (on 24 October) to 1650 millionths (on 30 October), indicating the emergence of new magnetic flux. The outlines of the coronal hole as observed on 26 and 30 October, 1992 are indicated in Figure 6 by the two superposed coronal-hole outlines.

The large low latitude coronal hole could be followed for at least six months after this time. It lay at S20° latitude but moved eastward in longitude by as much as 30° per solar rotation during these six months. This is in contrast to the behaviour of sunspots and other tracers of magnetic fields which normally remain fixed in heliographic longitude when they appear near 20° latitude. This observed rapid

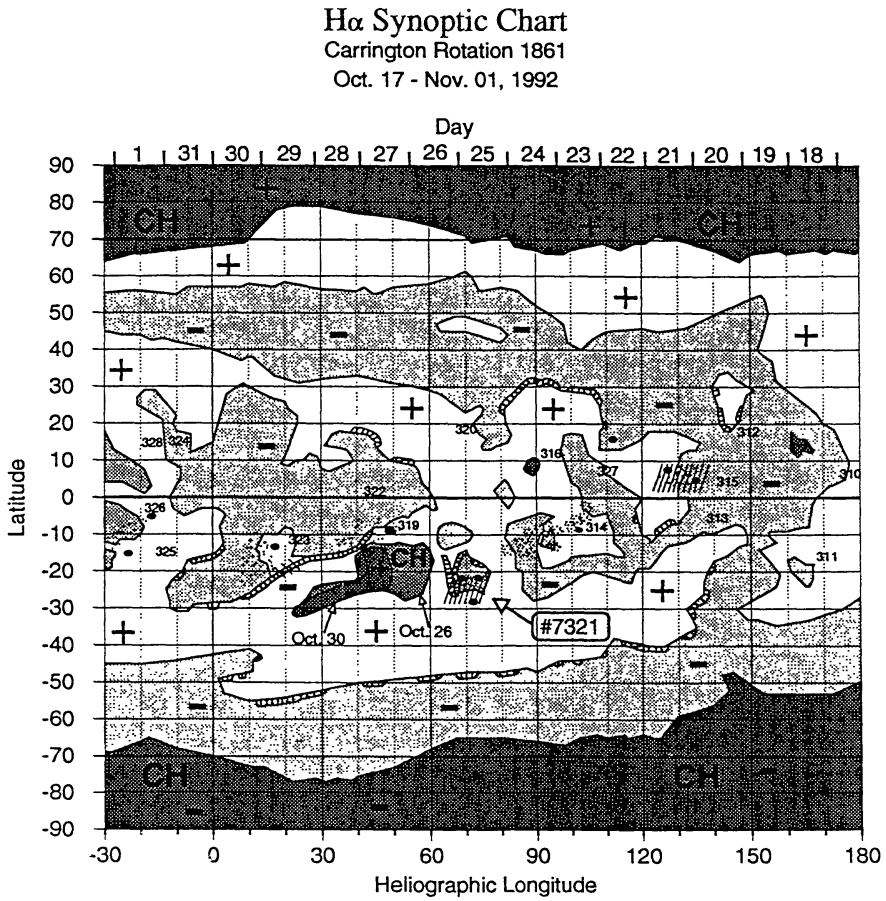

Figure 6. A partial Hα synoptic chart for Carrington rotation 1861 featuring NOAA region 7321 and showing the active regions, filaments and coronal holes (He I λ10830) nearby. Dates of central meridian passage at the top refer to the corresponding solar longitude at the bottom. Negative polarity is shaded light grey; positive polarity is white; coronal holes are dark grey and have the polarity of the surrounding solar surface. Large sunspots observed in Hα are large dots; bright chromospheric plages are areas of small dots; areas of diagonal lines overlying spots and plage indicate occurrence of strong X-ray flares. Dark filaments are irregular, cross hatched areas along some of the lines of polarity reversal near the important active region. This chart is substantially improved from the preliminary version published in the NOAA preliminary *Report and Forecast of Solar-Geophysical Activity*.

proper motion might account for part of the change in the eastern boundary of the coronal hole.

Another small, new coronal hole formed during this period, at heliographic latitude N 9° and longitude L 89°. This is marked 316 in Figure 6. This coronal hole, however, did not exhibit rapid changes during the period of interest to our observations.

Apart from the relatively rapid changes which had occurred at AR 7321 and the site of the coronal hole, there was filament activity also at AR 7321. Hα filtergrams, taken between 26 and 29 October, 1992, from the Udaipur Solar Observatory show a dark filament located between AR 7321 and the coronal hole at the east of the active region. On 30 October the filament had vanished. This is seen from Figure 7

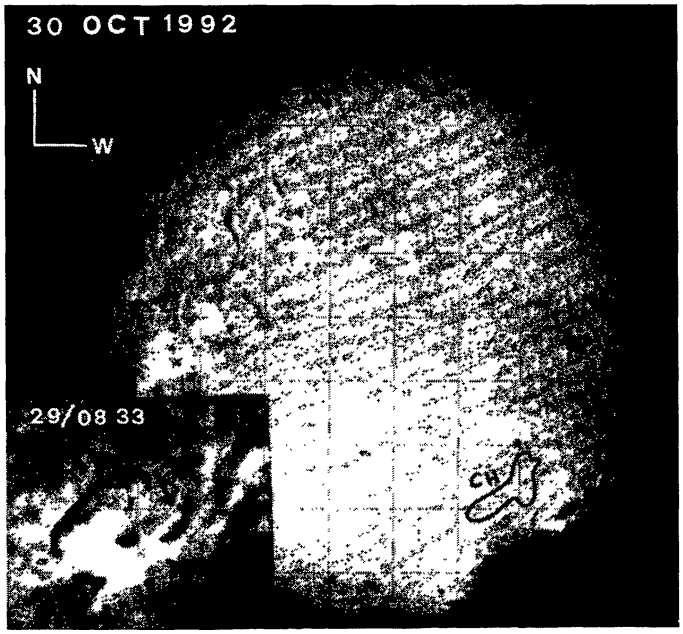

Figure 7. An Hα picture of the solar disk, on 30 October, showing the active region 7321. The region enclosed by the solid line and indicated by the letters CH marks the position of the coronal hole, while the active region is indicated by a small solid arrow and the letters AR. The inset is an enlarged portion of the active region, taken on 29 October, showing the dark Hα filament which is marked by the letter F and two small solid arrows.

which shows an Hα picture of the solar disc taken on 30 October, 1992. The inset in the figure is an enlargement of the active region, taken on 29 October, 1992, in which the dark filament is visible. The solid line in Figure 7 marks the boundary of the coronal hole.

7. Location and Source of the IP Disturbances

It is notable that there was so much activity on the solar surface on the few days immediately preceding the epoch of detection of travelling IP disturbances by IPS observations. Further, it is interesting that the activity involved flares and a filament eruption as well as a rapidly evolving coronal hole. In order to examine the connection between these solar surface activities and the observed travelling IP transients, we attempted to trace back the IPD to the solar surface by using the measured velocity of the IP disturbances. For this purpose it was assumed that the disturbance had propagated at a constant velocity equal to the velocity measured by the IPS observations, along the heliocentric radial line from the Sun to the point of closest approach of the LOS to the radio source. Such a simplifying assumption can lead to large uncertainties in the heliographic coordinates of the back-projected points, owing to the following reasons. Firstly, the solar wind velocity determined by IPS is a weighted average of the velocities at different points along the LOS to the source. This is due to the fact that the scattering power of the IP medium at

any point is a strong function of the distance from the Sun. Hence the maximum weighting is at a point on the LOS to the source which is closest to the Sun (point P in Figure 2). The weighting function decreases for the other points along the LOS on either side of point P. Secondly, the half width of the weighting function could be as large as 0.3 AU for a LOS at $\epsilon = 30°$, and would be larger for $\epsilon > 30°$ (Manoharan, 1991). Therefore, the single station IPS technique can underestimate the velocity of IP transients if they propagate along directions which deviate significantly from the radial line to the point of closest approach to the LOS.

Detailed estimates of the positional uncertainties in the back-projected points have not been made. However, from the scatter in the results obtained from computations for a large number of velocity measurements it appears that the positional uncertainties can be as large as a few tens of degrees in heliographic coordinates. It may be noted further that errors of ± 50 km s^{-1} in velocity give rise to uncertainties of only a few degrees in heliographic coordinates of the back projected points, for typical values of solar wind velocities. As such, the major cause for the large errors in the position of the back-projected points should be due to the fact that projection effects of the actual path of propagation of IP transients are not taken into account.

Albeit the positional errors, back-projection yields interesting insights on the solar sources of IPDs. The results from back projection of the data are shown in Figure 8. It covers a limited portion of the solar surface which is of interest. Points marked by large open circles correspond to velocity measurements greater than 600 km s^{-1} while the small filled circles represent lower velocity values. It is notable that most of the high velocity points project back to southern heliographic latitudes, indicating that the IPDs originated from activity in the southern solar hemisphere. On 31 October, 1992 most of the high velocity points trace back to locations in the longitude range 60° to 80°, which is the position of the active region AR 7321 (Figure 6). On 1 November, 1992 a significant number of high velocity points trace back to longitudes between 40° and 60°. This may be compared with the location of the contracted coronal hole lying between 25° and 50° longitudes. Recalling that the IPS observations detected the advancing front of the high velocities on 31 October, 1992 and the trailing edge of the high velocity disturbance on 1 November, 1992, the data of Figure 8 indicate that the high velocity front had its origin in the solar flare, and when the flare's contribution to the high velocity solar wind came to a close, the coronal hole adjacent to it sustained the high velocities. Comparison of data from 2 November in Figure 8 with the data for the preceding two days indicates that the solar wind had almost returned to its normal quiet state by 2 November. The high velocity points of 3 November, 1992 trace back to longitudes between 50° and 70°, and it is all quiet on 4 and 5 November, 1992. This being the case, the association of the high solar wind velocities observed on 3 November, 1992 with the flare of 2 November, 1992 is unambiguous.

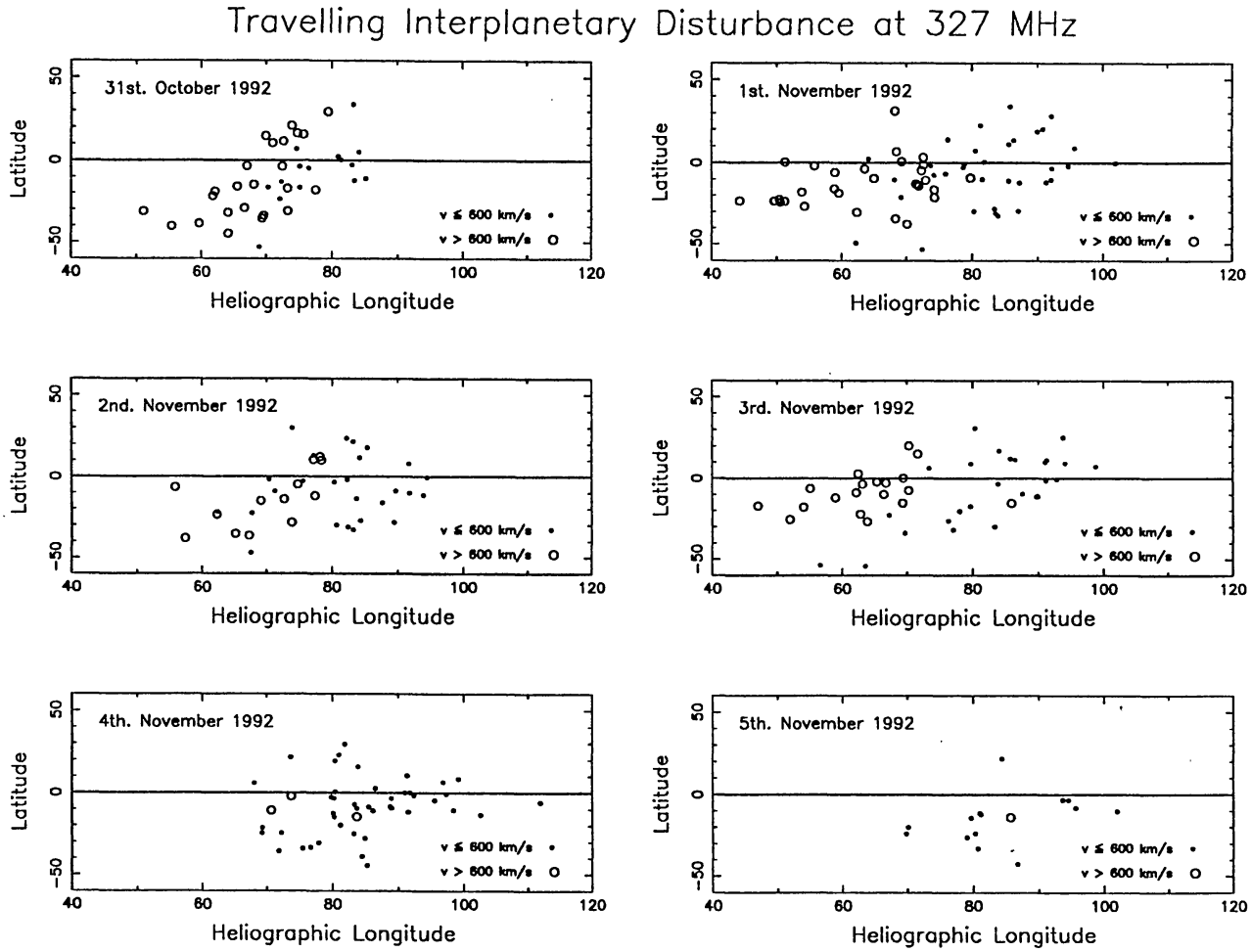

Figure 8. A scatter plot of solar wind velocities as a function of heliographic longitude (abcissa) and latitude (ordinate) for each of the six days of observation. The velocities are represented by two different markers with the small filled circles representing velocities $\leq$ 600 km s^{-1} and the open circles representing velocities $>$ 600 km s^{-1}.

8. Discussion and Conclusions

The observations and results reported here have relevance to several aspects of the origin and evolution of travelling IP disturbances as well as the methods of detecting them. It is important to note that two temporally distinct IP transients were predicted in advance by a theoretical model of propagation of IP shocks, on the basis of the observations of temporally separated events on the solar surface and both were detected unambiguously by using the technique of IPS. While this is not the first instance where IPS velocity observations have been traced back to solar events (Rickett, 1975; Jackson, Rompolt, and Švestka, 1988), these are the first observations where IPS has been used to obtain measurements with high enough spatial resolution to form an approximate image in the IPM of regions of high and low speed. The methodology adopted for detecting the IPDs was, in essence, the use of lines of sight to a set of spatially distributed compact radio sources as

a rapidly movable 'picket fence'. This was possible owing to the large collecting area and the steerability of the ORT. The ability to determine solar wind velocities reliably and rapidly has been particularly useful in the detection of the IP transients, and to some extent in tracing their origins at the solar surface. The full potential of the IPS data, however, was not realised in characterizing the IP transients due to two reasons. Firstly, the observations reported here were carried out during an IPS survey wherein the aim was to detect compact scintillating sources. As a result nearly 60% to 70% of the sources observed each day were non-scintillators which did not yield IPS spectra and hence velocities and g-values. Secondly, the g-maps produced did not have sufficient precision, due to a lack of a large number of observations on each scintillating source. It is hoped that both these problems will be solved after the IPS survey is complete and as more and more observations are obtained on each of the identified compact scintillating sources forming the 'picket fence'.

It may be noted that the discrepancies between the predicted and observed times of arrival of the IP disturbances are relatively minor. For example, the following changes in the inputs to the STOA model lead to precise agreement between the predicted and observed times of arrival of the IPD at the line of sight to the source, on 31 October, 1992:

- Same initial shock velocity (2000 km s^{-1}) as assumed earlier.
- Driver duration increased to 2.5 hours.
- Background solar wind speed increased to 500 km s^{-1}.

In retrospect, these changes to the input parameters of the STOA model appear quite reasonable. However, in view of the approximate nature of the STOA model which assumes the presence of a steady background solar wind in contrast to the reality of the possible existence of a pre-event, corotating, non-uniform solar wind structure, attempts at further fine-tuning the predictions of the model are not really warranted.

The proximity of the active region AR 7321 to the coronal hole, the rapid changes in their sizes, the filament eruption and the temporal sequence of the events observed on the surface of the Sun and the IP medium indicate that rapid rearrangement of magnetic fields had taken place before and after the flare event of 30 October. A possible scenario for the activity is suggested in Figures 9(a) and 9(b). Prior to the flare the configuration of the magnetic field and the location of the filament are indicated in Figure 9(a). The rapid emergence of new flux caused a decrease in size of the coronal hole and a corresponding increase in the size of the active region. The situation just after the flare is indicated in Figure 9(b). The flare caused the reconnection of the field lines thereby creating an open field configuration along which high speed streams could emanate. Also these high speed streams due to the flare and/or filament eruption would have enhanced the solar wind emerging from the neighbouring coronal hole, by flowing along the open field structure of the coronal hole. The scenario proposed above is in consonance with the ideas of Bravo and Pérez-Enríquez (1994). They have proposed that

the emergence of new flux of opposite polarity at an active region close to a coronal hole, could change the divergence of the flux lines from the coronal hole, with consequent increase in the velocity of the solar wind outflow from the hole. This sudden increase in velocity could subsequently generate a shock in the IP medium. They have considered a situation involving the increase in size of the base of the coronal hole, whereas our observations of the surface features on the Sun show that the size of the active region increased while that of the coronal hole decreased. The availability of reliable information on g-values would have helped in identifying whether the streams which crossed the LOS to the scintillating sources had enhanced or depleted density. In such a case it might have been possible to assess the relative contributions of the coronal hole and the flare-filament eruption combination to the observed high-speed stream. This is due to the fact that high velocity streams emanating from coronal holes are relatively tenuous compared to the normal solar wind plasma.

There are differing views regarding the association of IP transients (and also non-recurrent geomagnetic disturbances) with the type of solar surface phenomena. There have been studies which tend to associate most IPDs to transient mid-latitude coronal holes and a small fraction to regions on the Sun which are free of coronal holes as well as flares (Hewish and Bravo, 1986). Some of the drawbacks of these studies have been the coarse time resolution of the data, large errors in the determination of the velocity of propagation of the transients and contamination of data by ionospheric scintillation (Leinbach, Ananthakrishnan, and Detman, 1994). In a recent investigation involving advance prediction of a shock triggered by a flare and the detection of the associated IPD using IPS (Manoharan *et al.*, 1995) it was shown that the transient traced back to a flare site on the Sun; the coronal hole nearest to this site was more than 60° away in heliographic coordinates. Claim has also been made in recent times (Gosling, 1993) that non-recurrent geomagnetic storms and IPDs are generated solely due to coronal mass ejections (CME) and the role of flares in causing IPD and geomagnetic storms is secondary to that of CMEs.

In contrast to the above, the events described in this paper clearly show that both a flare and a coronal hole played key roles in generating the two separate IP transients. There is no data available regarding the occurrence or absence of a CME during the period of interest. However, the rapid changes which were observed on the solar surface prior to the event are indicative of large scale rearrangements of the magnetic fields in the region and hence the possibility that a CME might have occurred cannot be ruled out. Therefore, ruling out or supporting any particular phenomenon as the sole cause for IPDs and non-recurrent geomagnetic disturbances appears to be a bit premature. A much larger data base of observations providing both solar wind velocities and g-values, in conjunction with data on solar surface phenomena would be needed to reach firmer conclusions. In addition, collaborative, multi-station, IPS observations would be of considerable value.

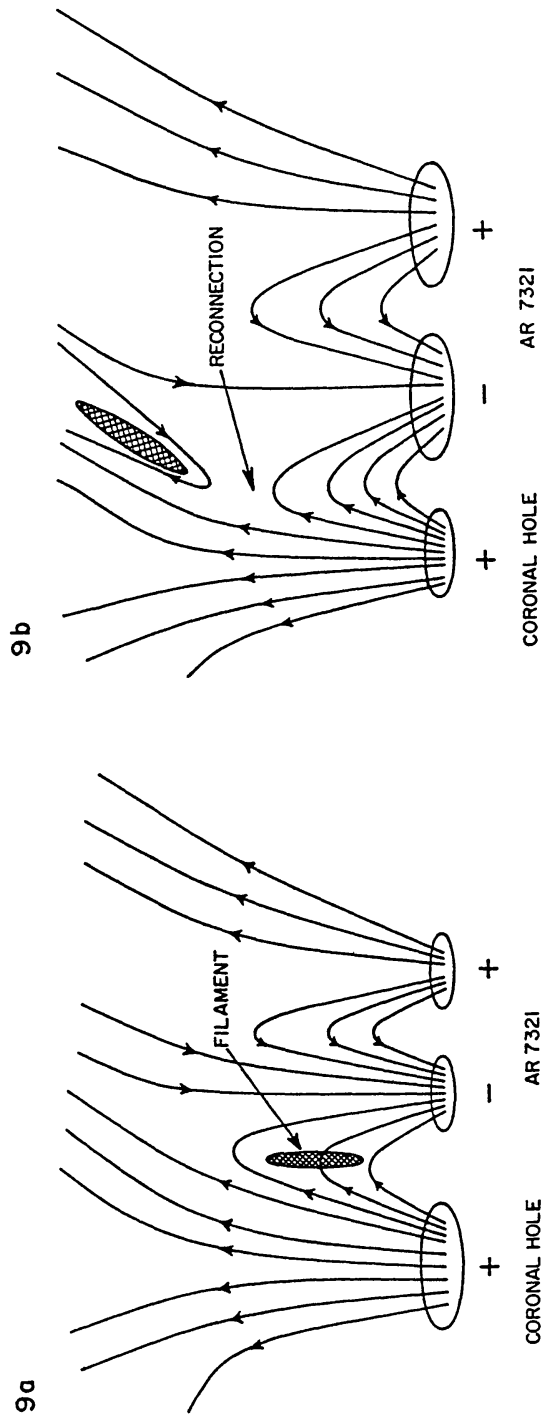

Figure 9. A schematic of the proposed scenario for the source of the two events from region 7321. (a) shows the active region 7321 and the coronal hole of predominantly positive polarity. Also shown by the small shaded region is the dark Hα filament (seen in Figure 7). (b) shows the scenario after the reconnection when the active region has enlarged greatly in area while the coronal hole has decreased in area.

Acknowledgements

One of the authors, JP, is grateful for a visiting fellowship at the Radio Astronomy Centre, during which this work was carried out. The work by MD was supported in part by a Naval Research Laboratory Contract No. N00173–93-WR30477. AB would like to acknowledge the support of an Indo–US collaborative project. The authors also wish to thank A. Hewish, E. Hildner, and S. Bravo for useful discussions, and P. K. Manoharan for use of the single station IPS software. The critical comments and corrections by the referee have significantly improved the clarity of this paper and we are happy to acknowledge it.

References

Alurkar, S. K., Bobra, A. D., Nirman, N. S., Venat, P., and Janardhan, P.: 1989, *Ind. J. Pure Appl. Phys.* **27**, 32.

Ananthakrishnan, S., Kulkarni, V. K., Ponsonby, J. E. B., Spencer, R. E., Graham, D. A., Porcas, R. W., Van Ardenne, A., Schilizzi, R. T., Gorgolewski, S., Kus, A., Matvyenko, L. I., and Papucenko, A. H.: 1989, *Monthly Notices Roy. Astron. Soc.* **237**, 341.

Balasubramanian, V., Janardhan, P., Ananthakrishnan, S., and Manoharan, P. K.: 1993, *Bul. Astr. Soc. India* **21**, 469.

Bird, M. K. and Edenhofer, P.: 1990, in R. Schwenn and E. Marsch (eds.), *Physics of the Inner Heliosphere I*, Springer-Verlag, Berlin, p. 13.

Bravo, S. and Pérez-Enríquez, R.: 1994, *Rev. Mexicana Astron. Astrofisica* **28**, 17.

Coles, W. A.: 1978, *Space Sci. Rev.* **21**, 411.

Dryer, M.: 1994, *Space Sci. Rev.* **67**, 363.

Gapper, G. R., Hewish, A., Purvis, A., and Duffett-Smith, P. J.: 1982, *Nature* **296**, 633.

Ghigo, F. D. and Owen, F. N.: 1978, Preprint No. 6, University of Texas Radio Astronomy Observatory.

Gosling, J. T.: 1993, *J. Geophys. Res.* **98**, No. A11, 18937.

Hewish, A. and Bravo, S.: 1986, *Solar Phys.* **106**, 185.

Hewish, A. and Duffett-Smith, P. J.: 1987, *Planetary Space Sci.* **35**, 487.

Hewish, A., Tappin, S. J., and Gapper, G. R.: 1985, *Nature* **314**, 137.

Jackson, B. V.: 1991, *Solar Wind Seven, Proc. 3rd COSPAR Colloquium*, p. 243.

Jackson, B. V., Rompolt, B., and Švestka, Z.: 1988, *Solar Phys.* **115**, 327.

Kakinuma, T., Washimi, H., and Kojima, M.: 1973, *Publ. Astron. Soc. Japan* **25**, 271.

Kakinuma, T. and Kojima, M.: 1984, *Proc. Res. Inst. Atmos.* **31**, 1.

Large, M. I., Mills, B. Y., Little, A. G., Crawford, D. F., and Sutton, J. M.: 1981, *Monthly Notices Roy. Astron. Soc.* **194**, 693; and Microfiches MN 194/1.

Leinbach, H., Ananthakrishnan, S., and Detman, T. R.: 1994, NOAA Tech. Memo. ERL SEL-83.

Manoharan, P. K.: 1991, PhD Thesis, Bombay University, India.

Manoharan, P. K. and Ananthakrishnan, S.: 1990, *Monthly Notices Roy. Astron. Soc.* **244**, 691.

Manoharan, P. K., Ananthakrishnan, S., and Pramesh Rao: 1987, *Proc. of the Sixth Solar Wind Conf.* Vol. I, p. 55.

Manoharan, P. K., Ananthakrishnan, S., Dryer, M., Detman, T. R., Leinbach, H., Kojima, M., Watanabe, T., and Kahn, J.: 1995, *Solar Phys.* **156**, 377.

Marians, M.: 1975, *Radio Sci.* **10**, 115.

Rickett, B. J.: 1975, *Solar Phys.* **43**, 237.

Salpeter, E. E.: 1967, *Astrophys. J.* **147**, 433.

Schwenn, R.: 1986, *Space Sci. Rev.* **44**, 139.

Scott, S. L., Coles, W. A., and Bourgeois, H.: 1983, *Astron. Astrophys.* **123**, 207.

Selvanayagam, A. J., Praveenkumar, A., Nandagopal, D., and Velusamy, T.: 1993, *IETE Technical Rev.* **10**, No. 4. 333.

Smart, D. F. and Shea, M. A.: 1985, *J. Geophys. Res.* **90**, 183.
Smart, D. F., Shea, M. A., Dryer, M., Quintana, L. C., Gentile and Bathurst, A. A.: 1986, in P. A. Simon, G. R. Heckman, and M. A. Shea (eds.), *Solar-Terrestrial Predictions*, U.S. Govt. Printing Office, Washington, p. 471.
Smith, Z. and Dryer, M.: 1990, *Solar Phys.* **129**, 387.
Smith, Z. and Dryer, M.: 1991, *Solar Phys.* **131**, 363.
Watanabe, K. and Marubashi, K.: 1985, *J. Geomag. Geoelectr.* **37**, 869.
Woo, R. and Armstrong, J. W.: 1981, *Nature* **292**, 608.
Yakovlev, O. I., Efimov, A. I., Razmanov, V. M., and Shtrykov, V. K.: 1980, *Soviet Astron.* **24**, 454.